Supporting Information for

# Microenvironments of Cu Catalyst in Zero-gap Membrane Electrode Assembly for Efficient $CO_2$ Electrolysis to $C_{2+}$ Products

Woong Choi‡, Yongjun Choi‡, Eunsuh Choi, Hyewon Yun, Wonsang Jung, Woong Hee Lee, Hyung-Suk Oh, Da Hye Won, Jonggeol Na,* and Yun Jeong Hwang*

## Supplemental Method

### Calculation of Faradaic efficiency

Partial currnet density of each product ($i_{product}$) was calculated by substituting the volume concentration ($c_{product}$) of each gaseous and liquid product, which were obtained from gas chromatograms and NMR, into the following equation.

$$i_{product} = c_{product} \times n_{product} \times \frac{vFp_0}{RT}$$

where $n_{product}$ is number of electrons to yield each product from $eCO_2RR$, v, F, p0, R, and T represent flow rate, Faradaic constant, gas pressure in MEA cell, ideal gas constant, and temperature, respectively.

In addition, Faradaic efficiency for each product ($FE_{product}$) was calculated from the ratio between total current and partial current of each product as follow.

$$FE_{product} = \frac{i_{product}}{i_{total}} \times 100$$

Where $i_{total}$ means measured total current density

### Calculation of energy efficiency (EE)

EEs for total $eCO_2RR$ and $C_{2+}$ production for each catalyst were calculated based on the recorded applied cell potential ($E$) and FEs for each product ($^{FE_i}$) using following equations.

$$EE_i = \frac{E_i^o}{E} \times FE_i$$

$$EE_{total\ CO2RR} = \sum_i EE_i$$

Where $E_i^o$ represents standard reduction potential of each product from $CO_2$ coupling with standard reduction potential of oxygen evolution reaction. $EE_{C2+product}$ contains ethylene, ethanol, acetate, and propanol.

### Electrochemical active surface area (ECSA) measurement

The ECSA of each Cu catalyst was measured by under-potential deposition (UPD) of Pb referring previous report.[1] Each Cu-0, pCu, and Cu-5 electrode was fabricated by a loading 0.5 mg $cm^{-2}$ on carbon paper (Sigracet 39BB) with 1 $cm^2$ electrode area. For the electrochemical measuremenets, 3 M Ag/AgCl and Pt plates were employed as a reference and counter electrode, respectively. Before the Pb-UPD, Cu catalyst electrodes were reduced at -3.0 V (vs. 3 M Ag/AgCl) in $N_2$ bubbled 0.1 M $HClO_4$ solution for 10 min. Subsequently, a cyclovoltametry from -0.1 V to -0.5 V with 10 mV $s^{-1}$ scan rate was performed in $N_2$ bubbled 0.001 M $Pb(ClO_4)_2$ and 0.1 M $HClO_4$ aqueous electrolyte

### Computational fluid dynamics simulation

In order to theoretically confirm how the device performance (e.g., Faraday efficiency) changes according to the thickness of the catalyst layer, we developed a device model that considers various transport phenomena such as diffusion and migration through potential fields. We employed finite-element methods (FEM) based computational fluid dynamics (CFD) with commercial software COMSOL Multiphysics® version 5.6 (https://www.comsol.com/) with 'Fuel cell & electrolyzer' module under 16 cores of Intel Xeon Gold 6242 (2.8 GHz) processors. Multifrontal massively parallel sparse direct solver (MUMPS) was used and multi-

step approach, which varies applied cell potential from 2.0 V to 4.0 V (or target potential) with 0.01 V step-size, was also used. Important governing equations are (1) solid phase electric potential,

$$\nabla \cdot i_s = -\sum_k a_{s,k} i_k$$

$$i_s = -\sigma_s^{eff} \nabla \phi_s$$

where $i_s$ is electrode current density, $i_k$ is partial current density of reaction k, $a_{s,k}$ is specific surface area for reaction k assumed same for every charge transfer reactions, $\sigma_s$ is electronic conductivity, $\phi_s$ is electronic potential for solid phase. (2) Liquid phase electric potential is connected to solid phase electic potential as,

$$\nabla \cdot i_L = -\nabla \cdot i_s$$

where $i_L$ is electrolyte current density. Mass fraction of gas species can be expressed as,

$$\nabla \cdot n_i = R_{Phase\ Transfer,i} + R_{Bulk,i} + R_{Charge\ Transfer,i}$$

$$n_i = -\rho_G D_i^{eff} \nabla \omega_i - \rho_G D_i^{eff} \omega \frac{\nabla M_n}{M} + \rho_i u_G$$

$$\sum_i \omega_i = 1$$

where $n_i$ is mass flux of gas species i, $R_{Phase\ Transfer,i}$ is phase transfer rate for species i, $R_{Bulk,i}$ is bulk reaction rate for species i, $R_{Charge\ Transfer,i}$ is charge transfer reaction rate for species i, $D_i$ is diffusivity of species i, $\rho$ is mass density, $\omega_i$ is mass fraction of species i, and u is mass-averaged fluid velocity. (3) Ionic species mass fraction is almost same as neutral species but we should include migration through electric field expressed as,

$$\nabla \cdot n_j = R_{Phase\ Transfer,j} + R_{Bulk,j} + R_{Charge\ Transfer,j}$$

$$n_j = -\rho_L D_j^{eff} \nabla \omega_j + \frac{\rho_L D_j^{eff} \omega_j z_j F}{RT} \nabla \phi_L$$

$$\sum_j \frac{z_j \omega_j}{M_j} = 0$$

where $n_j$ is mass flux of ionic species j, $z_j$ is charge of species j, $\xi$ is electro-osmotic coefficient, and superscript $eff$ means effective property. (4) Liquid water mass fraction can be expressed as

$$n_{H_2O} = -\rho_L D_{H_2O}^{eff} \nabla \omega_{H_2O} + \sum_j \frac{\xi_j^{eff} n_j}{M_j}$$

, and transport mechanisms are governed by Maxwell-Stefan diffusion equation, diffusion-effective diffusivity model for porous media is governed by Bruggeman model, and migration in electric field is governed by Nernst-Einstein relation.

We have to consider various charge transfer reactions that can cover HER, $C_1$, and $C_2$ to extract the trend of $C_{2+}$ FE. Thus, we employed one charge transfer reactions (OER on $IrO_2$) at the anode and four charge transfer reactions (reduction reactions to produce $H_2$, CO, $C_2H_4$, $C_2H_5OH$ on the proposed Cu-5 catalyst) at the cathode based on the Butler-Volmer equation,

$$i_k = i_{o,k}\prod_j\left(\frac{c_j}{c_j^{ref}}\right)^{\gamma_{j,k}} \cdot \exp\left(-\frac{\alpha_{c,k}F}{RT}\eta_k\right)$$

$$\eta_k = (\phi_s - \phi_L) - \left(U_k^o - \frac{(\ln 10)\times RT}{F}pH\right)$$

where $i_o$ is exchange current density, $c_j$ is activity of species j, $\gamma_k$ is reaction order with respect to species j for reaction k, $\alpha_{c,k}$ is cathodic transfer coefficient of reaction k, $\eta_k$ is surface overpotential for reaction k, and $U_k^o$ is reference potential of reaction k. The list of reactions are

| Product | Reactions |
|---|---|
| **Anode** | |
| $O_2$ | $4OH^- \rightarrow O_2 + 2H_2O + 4e^-$ |
| **Cathode** | |
| $H_2$ | $2H_2O + 2e^- \rightarrow H_2 + 2OH^-$ |
| CO | $CO_2 + H_2O + 2e^- \rightarrow CO + 2OH^-$ |
| $C_2H_4$ | $2CO_2 + 8H_2O + 12e^- \rightarrow C_2H_4 + 12OH^-$ |
| $C_2H_5OH$ | $2CO_2 + 9H_2O + 12e^- \rightarrow C_2H_5OH + 12OH^-$ |

where reference potential, exchange current density, charge transfer coefficient, and chemical activity of each reaction are shown in Table S1. Reference potential and chemical activity of each reaction are from Weng et. al.[2], and exchange current density and charge transfer coefficient are fitted by the partial current density of electron transfer limited $H_2$, CO, $C_2H_4$, and liquid products (represented to $C_2H_5OH$) production reactions measured at -3.00 to -4.00 V (vs. RHE) Cu-5 where experimental data is Fig. 2c and fitting results are shown in Fig. 3b. Our target objective function is mean squared error between experimental FE and simulated FE, and we tried to minimize it. Parameter estimated proposed model was able to predict the results of the FE and total current density according to the applied cell potential ($E_{cell}$).

For ions in electrolyte and chemical species, $H^+$, $HCO_3^-$, $CO_3^{2-}$, $OH^-$, $CO_2$, CO, $C_2H_4$, $H_2$, $O_2$, $H_2O$, and $C_2H_5OH$ were defined as mixture fluid material with each diffusion coefficient. In the case of homogeneous reactions, we considered volume reactions of carbonate equilibria[3-5] and water self-ionization[3,6] for rigorous dynamic responses of electrochemical reaction rates and transport effects of various species simultaneously. The equations and all physical properties and parameters used in the model are summarized in Supplementary Table 1.

| | |
|---|---|
| carbonate equilibria - 1 | $CO_2(aq) + OH^-(aq) \rightleftharpoons HCO_3^-(aq)$ |
| carbonate equilibria - 2 | $HCO_3^-(aq) + OH^-(aq) \rightleftharpoons CO_3^{2-}(aq) + H_2O(l)$ |
| water self-ionization | $H^+(aq) + OH^-(aq) \rightleftharpoons H_2O(l)$ |

In Fig. 3a, a schematic of the simulation domain boundary used for the thickness effect study is shown. A four-layered structure consisted of the anode (Pt-Ti mesh, 270 μm), the membrane (70 μm), catalyst (we set the thickness of catalyst layer as variable), and the cathode (carbon paper (Sigracet 39bb), 300 μm) were considered and all domain were fully defined in CFD simulation. Particularly, boundary conditions between bulk electrolyte solution (0.1 M $KHCO_3$) and anode (Fig. 3a, boundary (I)) were

| | |
|---|---|
| $c_i = 0$ | Zero concentration of gas species |
| $c_{j \neq CO_2} = 0.1\ M\ KHCO_3\ solution$ | Concentration of other species are calculated by fleshly prepared 0.1 M $KHCO_3$ solution (pH ≈ 8.34) |
| $\phi_s = E_{cell}$ | Applied cell potential (we can vary this) |

Boundary conditions of the anode-membrane and membrane-catalyst (Fig. 3a, boundary (II and III)) were

| | |
|---|---|
| $n_i$ | Zero flux for gaseous species |

Boundary conditions of the catalyst-cathode (Fig. 3a, boundary (IV)) were

| | |
|---|---|
| $n_j$ | Zero flux for ionic species |

Finally, boundary conditions of cathode-humidified $C_O2$ gas chamber Fig. 3a, boundary (V)) were

| | |
|---|---|
| $y_{CO_2}$ | $1 - y_{H_2O}$ |
| $y_{H_2O}$ | $0.99 \times \frac{P_{sat}}{P_{atm}}$ (99% relative humidity) |
| $\phi_s = 0$ | Arbitrary reference potential |

**Table S1** Rate parameters for charge transfer reactions

| | $U_k^o$ (V) | $i_{o,k}$ (mA/cm$^2$) | $\alpha_{a/c,k}$ | $\prod_j \left(\frac{c_j}{c_j^{ref}}\right)^{\gamma_{j,k}}$ |
|---|---|---|---|---|
| **OER on $IrO_2$** | | | | |
| O2 (acid) | 1.23 | $1.2 \times 10^{-8} exp\left(-\frac{0.01[eV]pH}{k_B T}\right)$ | 1.5 | $a_w^{1.6}$ |
| **HER & CO2R on Cu-5** | | | | |
| $H_2$ | 0 | $7 \times 10^{-11} exp\left(-\frac{0.01[eV]pH}{k_B T}\right)$ | 0.4 | $a_w^2$ |
| CO | −0.11 | $1.3 \times 10^{-2}$ | 0.14 | $a_w \left(\frac{[CO_2]}{1M}\right)^{1.50}$ |
| $C_2H_4$ | 0.07 | $9.5 \times 10^{-6}$ | 0.24 | $a_w^3 \left(\frac{[CO_2]}{1M}\right)^{1.36}$ |
| $C_2H_5OH$ | 0.08 | $1.2 \times 10^{-4}$ | 0.17 | $a_w^3 \left(\frac{[CO_2]}{1M}\right)^{0.96}$ |

**Table S2** Physical properties and model parameters for CFD simulations.

| Input parameter | Reference | Description | Value |
|---|---|---|---|
| $L_{anode}$ / m | experiment | The thickness of the anode Pt-Ti mesh layer | $2.7\times10^{-4}$ |
| $L_{membrane}$ / m | experiment | The thickness of the membrane layer | $7.0\times10^{-5}$ |
| $L_{catalyst}$ / m | variable | The thickness of the catalyst layer | - |
| $L_{cathode}$ / m | experiment | The thickness of the cathod carbon paper layer | $3.0\times10^{-4}$ |
| $D_{particle}$ / m | experiment | The diameter of pseudo-particle of catalyst layer | $2.85\times10^{-7}$ |
| $\varepsilon_{catal,\ cathode}$ | experiment | Pseudo-porosity of catalyst layer and cathode | 0.627 |
| $\varepsilon_{anode}$ | [7] | Pseudo-porosity of anode Pt-Ti mesh | 0.8 |
| $\sigma_{catal}$ / S m$^{-1}$ | [7] | Electronic conductivity in catalyst layer | 220 |
| $\sigma_{cathode}$ / S m$^{-1}$ | [7] | Electronic conductivity in cathode diffusion medium (carbon paper) | 100 |
| $a_V$ / m$^{-1}$ | experiment | Active specific surface area | $1.958\times10^{8}$ |
| $[CO_2]_{bulk\text{-}anode}$ / M | | 25 °C 0.1 M $KHCO_3$ solution | 0 |
| $[H^+]_{bulk\text{-}anode}$ / M | | 25 °C 0.1 M $KHCO_3$ solution | $4.57\times10^{-9}$ |
| $[HCO_3^-]_{bulk\text{-}anode}$ / M | | 25 °C 0.1 M $KHCO_3$ solution | $9.90\times10^{-2}$ |
| $[CO_3^{2-}]_{bulk\text{-}anode}$ / M | | 25 °C 0.1 M $KHCO_3$ solution | $1.01\times10^{-3}$ |
| $[OH^-]_{bulk\text{-}anode}$ / M | | 25 °C 0.1 M $KHCO_3$ solution | $2.19\times10^{-6}$ |
| $k_1$ | [3,4] | Forward kinetics coefficient of carbonate equilibria - 1 | $5.93\times10^{3}$ |
| $k_{-1}$ | [3,4] | Reverse kinetics coefficient of carbonate equilibria - 1 | $1.36\times10^{-4}$ |
| $k_2$ | [3,4] | Forward kinetics coefficient of carbonate equilibria - 2 | $1.00\times10^{8}$ |
| $k_{-2}$ | [3,4] | Reverse kinetics coefficient of carbonate equilibria - 2 | $2.15\times10^{4}$ |
| $k_w$ | [3,6] | Forward kinetics coefficient of water self-ionization | $1.40\times10^{11}$ |
| $k_{-w}$ | [3,6] | Reverse kinetics coefficient of water self-ionization | $1.40\times10^{-3}$ |

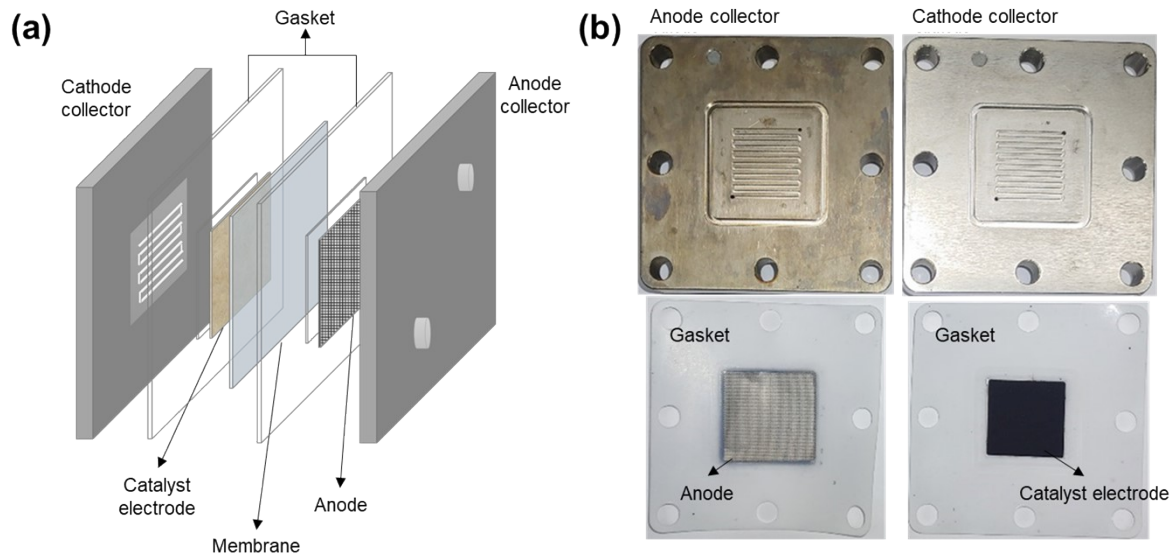


**Fig. S1** (a) Schematic image of MEA electrolyzer configuration. (b) Images of each compartments of MEA electrolyzer.

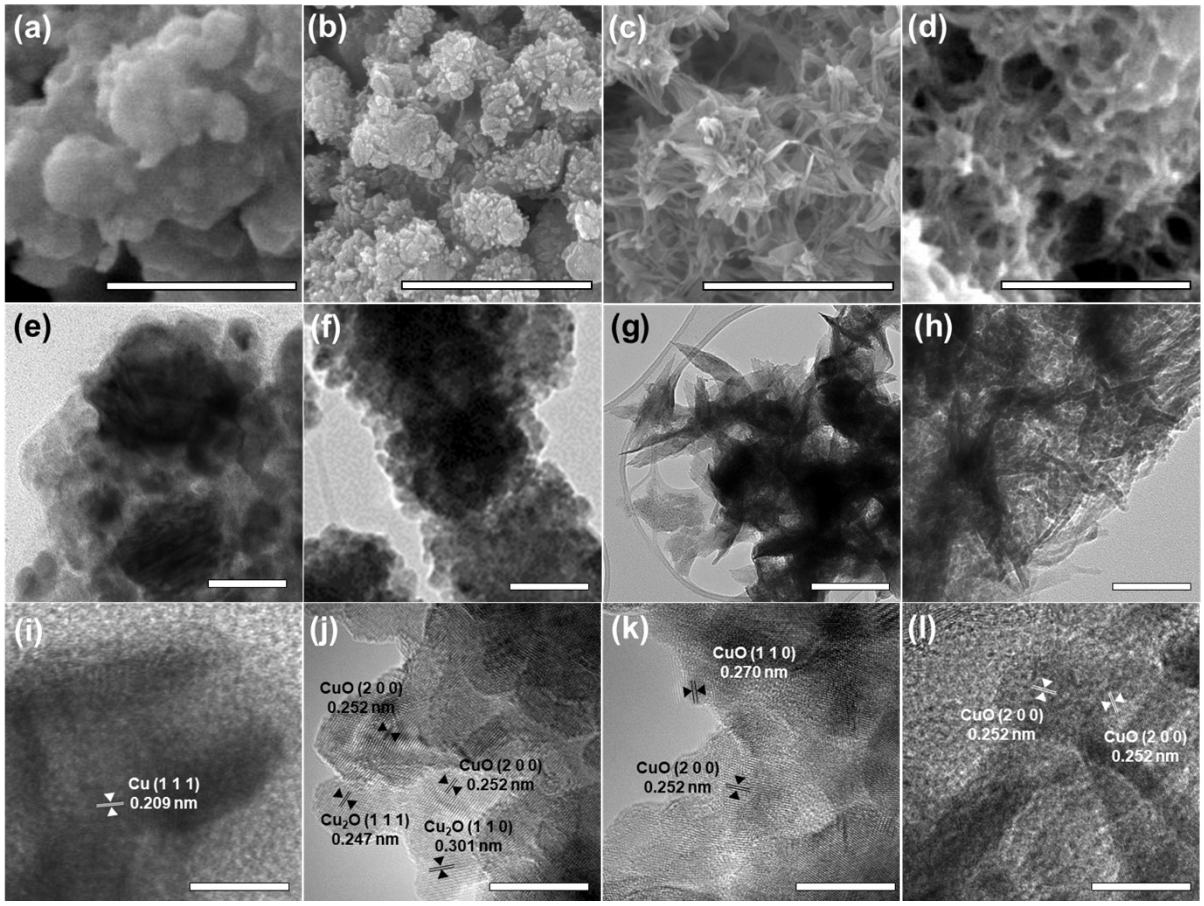


**Fig. S2** SEM, TEM, and HRTEM images of Cu nanoparticles after (a,e,i) 0 h, (b,f,j) 1 h, (c,g,k) 5 h, and (d,h,k) 12 h KOH treatments. Scale bars represent (a,b,c,d) 500 nm, (e,f,g,h) 50 nm, and (i,j,k,l) 10 nm.

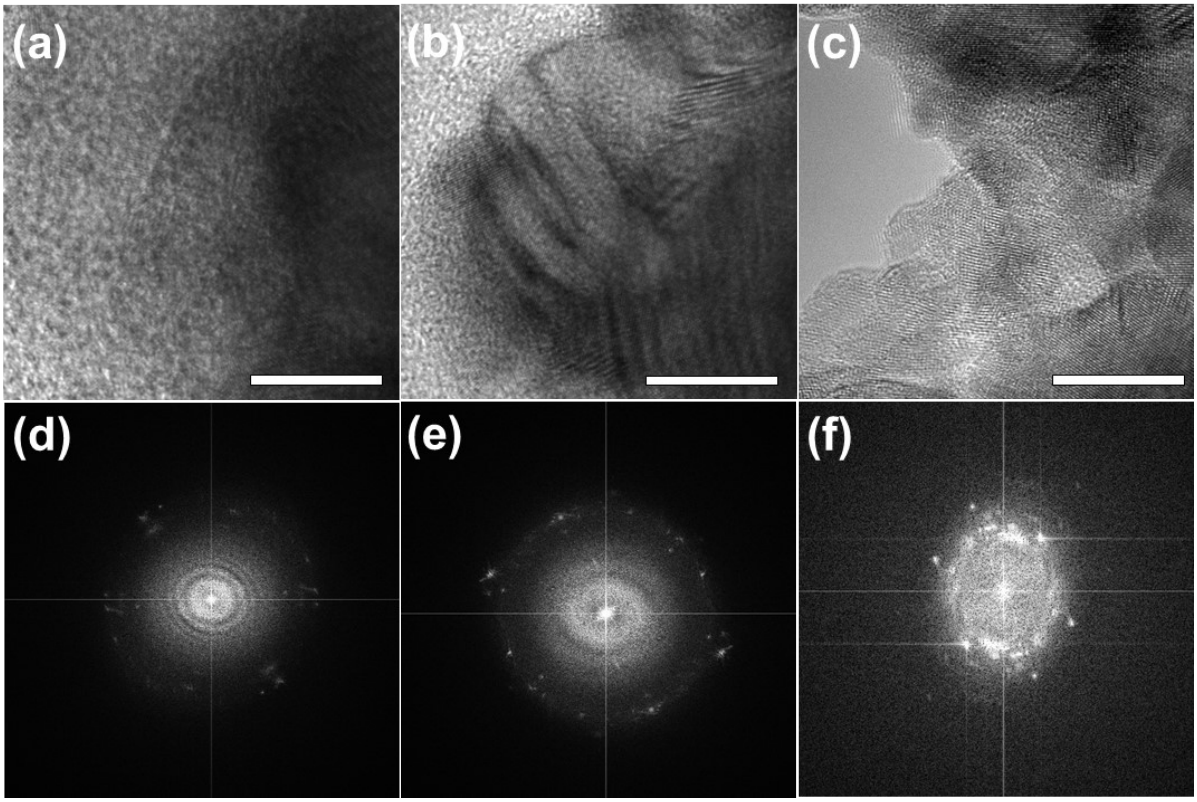


**Fig. S3** (a,b,c) HRTEM images of (a) Cu-0, (b) pCu, and (c) Cu-5. The bars represented 10 nm. (d,e,f) FFT patterns of (d) Cu-0, (e) pCu, and (f) Cu-5.

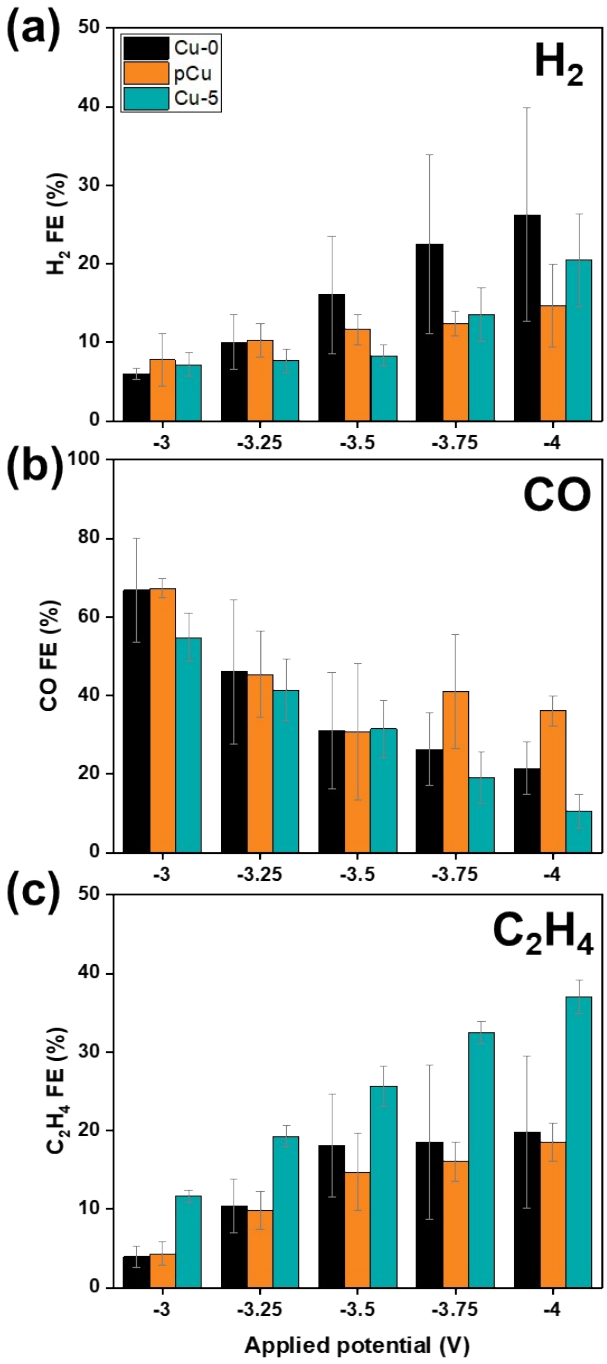


**Fig. S4** (a) $H_2$, (b) CO, and (c) $C_2H_4$ FEs of Cu-0 (black), pCu (orange), and Cu-5 (dark cyan) at each applied cell potential. Error bars represent standard deviations of 3-5 times individual experiments.

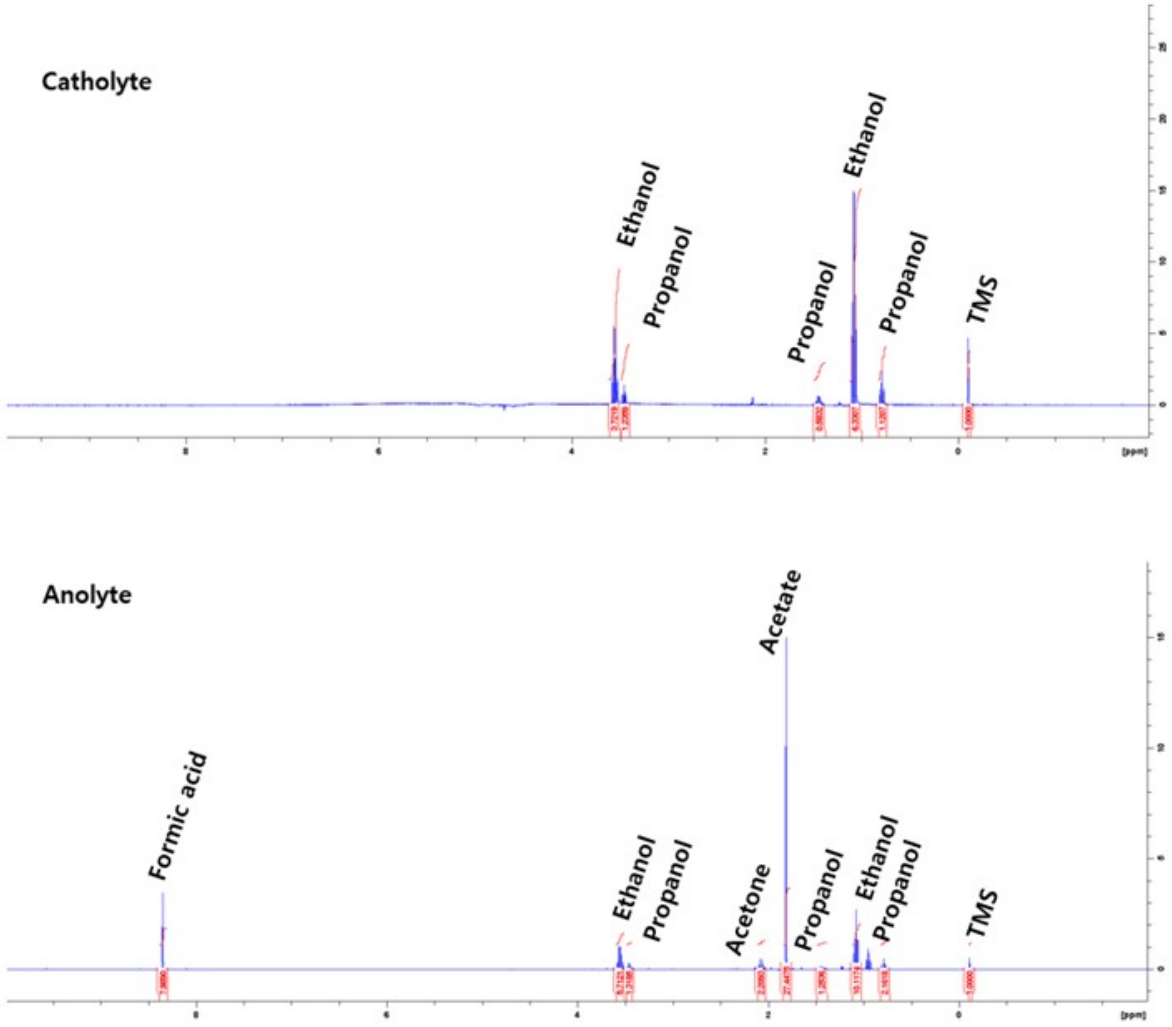


**Fig. S5** Representative $^{1}H$ NMR spectra of the anolyte and the captured $CO_2$ outflow using the cold trap, respectively after the $eCO_2RR$ with the MEA cell. TMS was used as an internal standard.

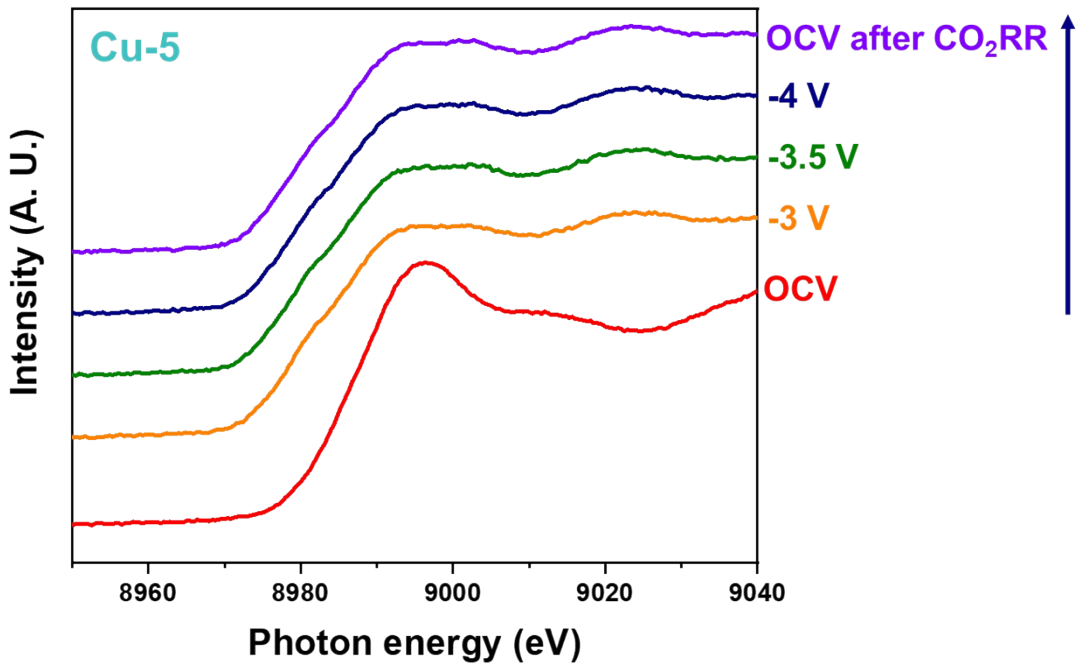


**Fig. S6** In-situ XANES spectra of Cu-5 catalyst in MEA cell during e$CO_2$RR at stepwise applied cell potential. All reaction conditions were identical to a general e$CO_2$RR in MEA cell. Spectrum were obtained after 10 min operation at each applied potential, and the applied potential was switched after 30 min.

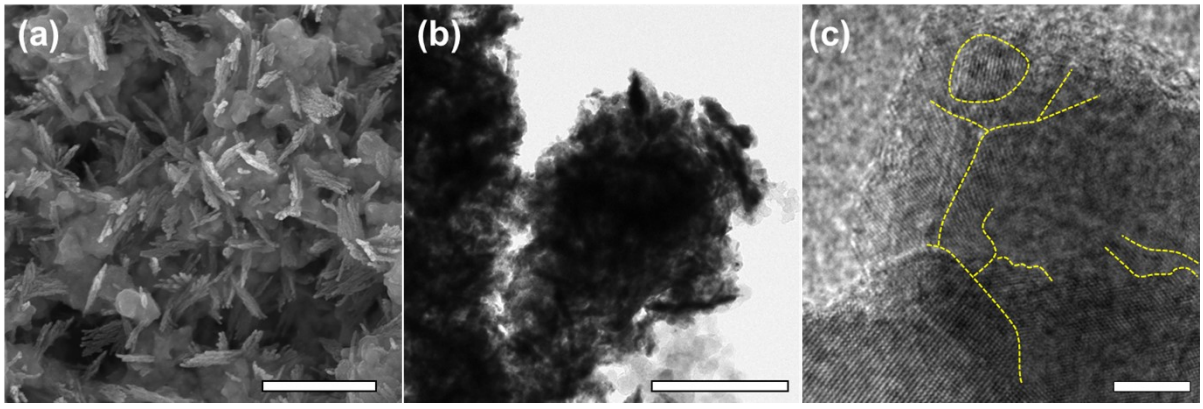


**Fig. S7** (a) SEM, (b) TEM, and (c) HRTEM images of Cu-5 catalyst after the stepwised $eCO_2RR$ in MEA cell. The yellow dash lines in HRTEM image show the grain boundaries of small Cu domains. The bars represent (a,b) 500 nm and (c) 5 nm, respectively.

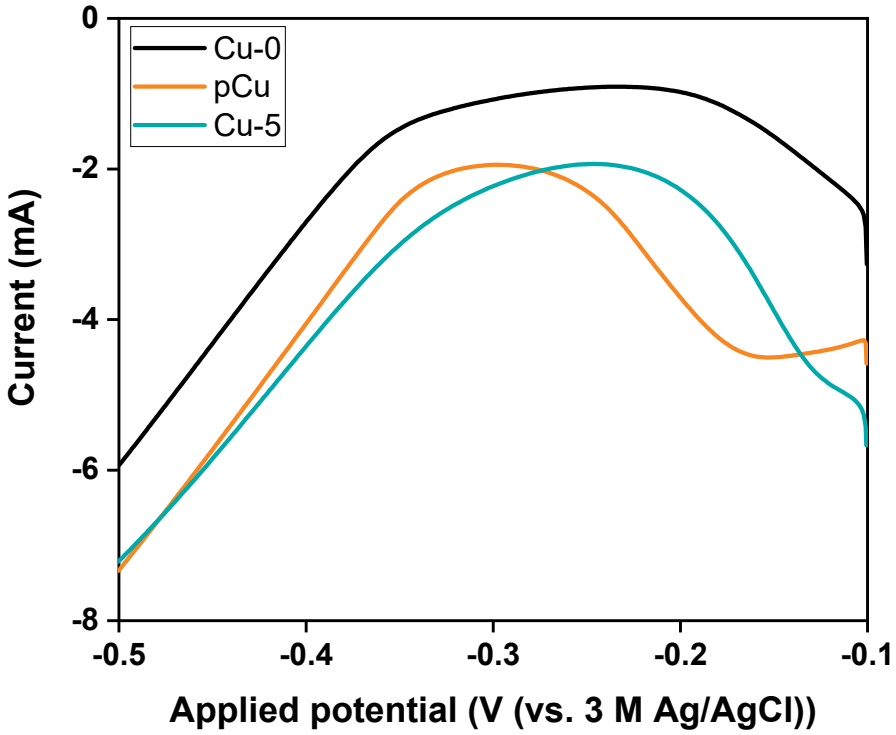


**Fig. S8** Cyclo-voltametry (CV) curves of Cu-0 (black), pCu (orange), and Cu-5 (dark cyan) for electrochemical active surface area (ECSA) measuremts. CV curves were obtained from -0.1 V to -0.5 V under $O_2$-free 0.001 M $Pb(ClO_4)_2$ and 0.1 M $HClO_4$ aqueous electrolyte and 10 mV s-1 scan rate.

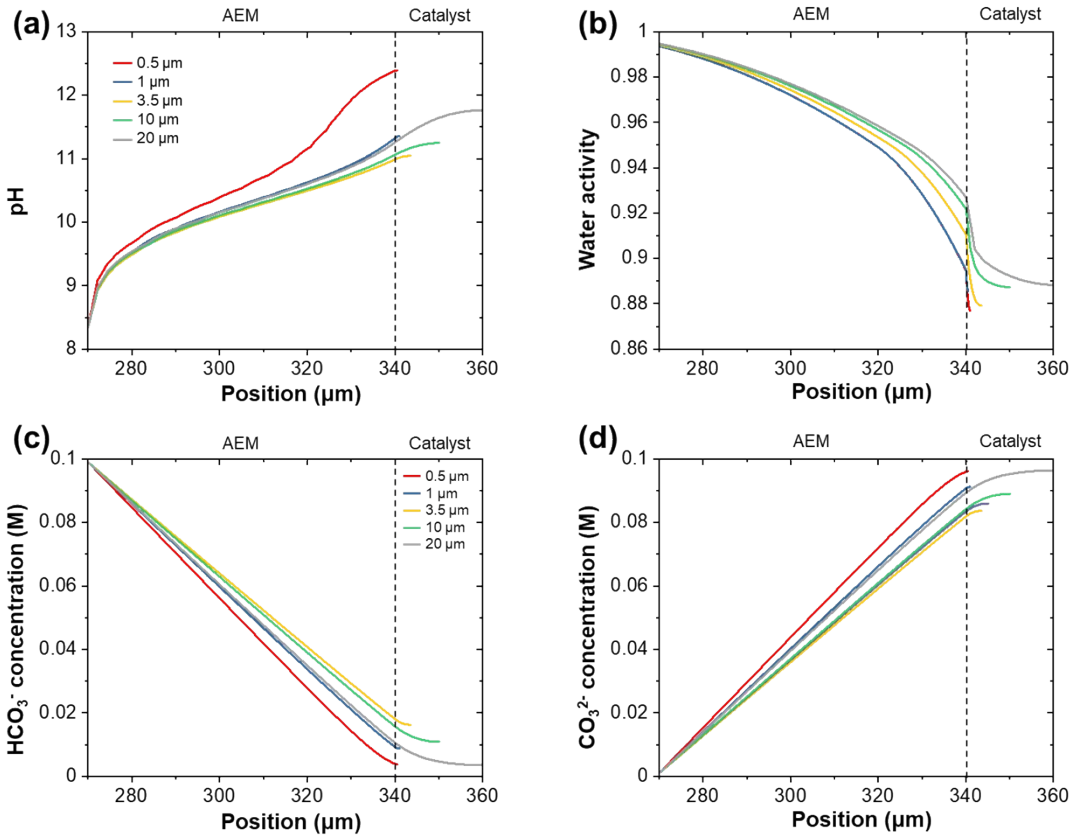


**Fig. S9** Computational results of the catalyst thickness effect for extrinsic properties (a) pH, (b) water activity, (c) bicarbonate ion concentation, and (d) carbonate ion concentration.

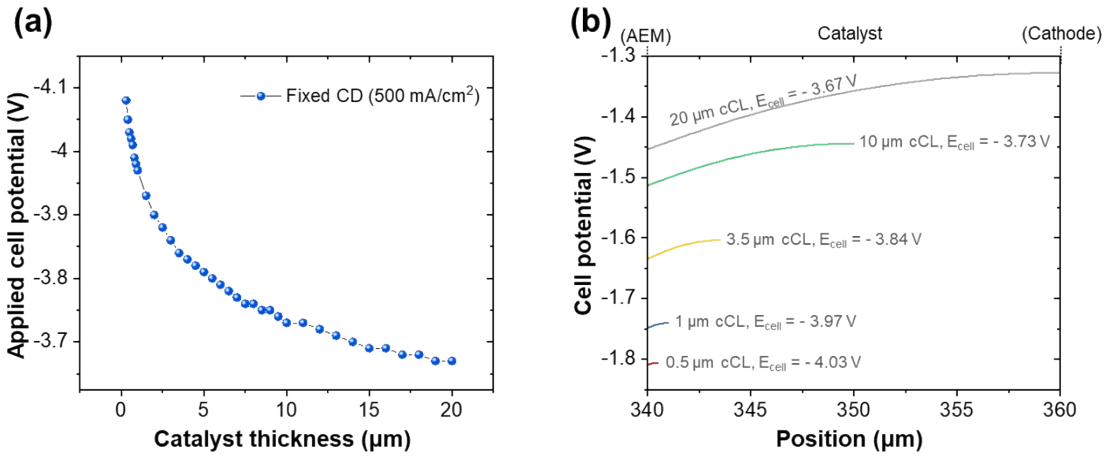


**Fig. S10** (a) The required applied cell potential and (b) the local cathode potential (vs. RHE) to maintain fixed current density as 500 mA/cm$^2$ at different thickness cathode catalyst layer.

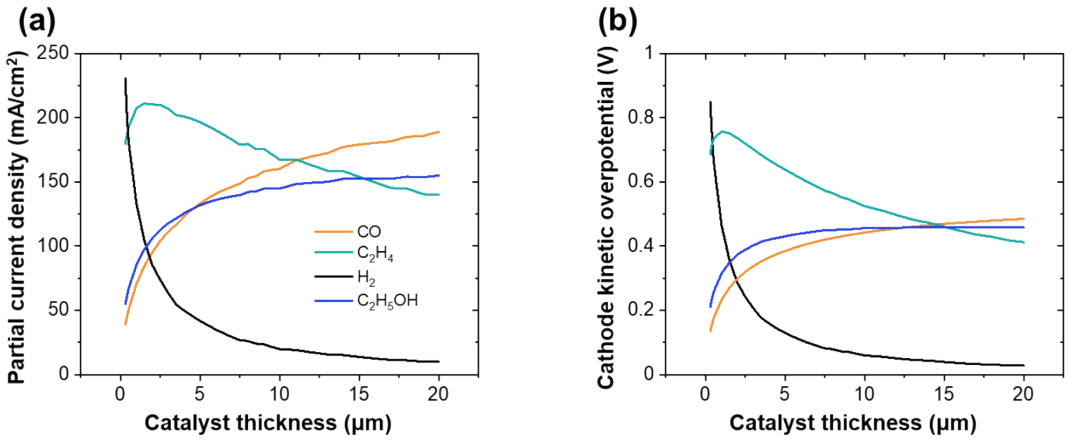


**Fig. S11** Plots of (a) partial current density and (b) cathode kinetic overpotential at the fixed current density (500 mA/cm$^2$) as a function of catalyst layer thickness.

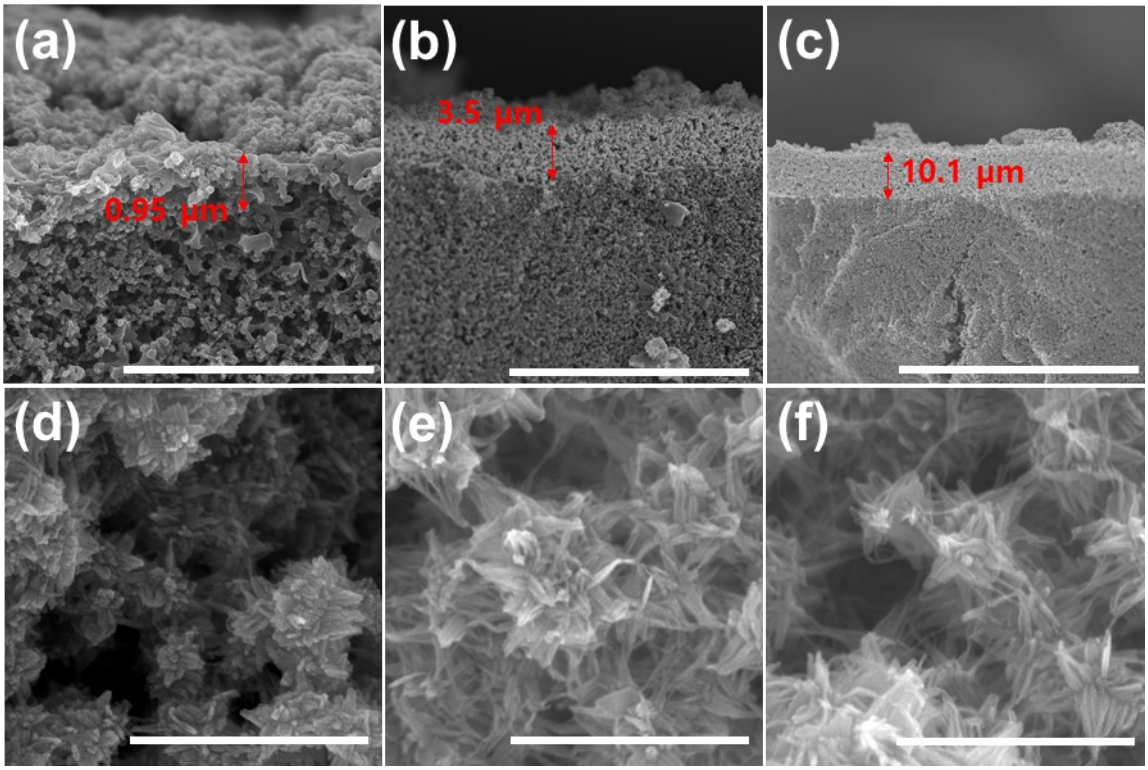


**Fig. S12** (a,b,c) Cross-sectional SEM images of (a) Cu-5-1, (b) Cu-5-3 and (c) Cu-5-10. The bars represent (a) 4 μm, (b) 20 μm, and (c) 50 μm, respectively. (d,e,f) SEM images of (d) Cu-5-1, (e) Cu-5-3 and (f) Cu-5-10. The bars represent (a) 4 μm, (b) 20 μm, (c) 40 μm, and (d,e,f) 500 nm, respectively.

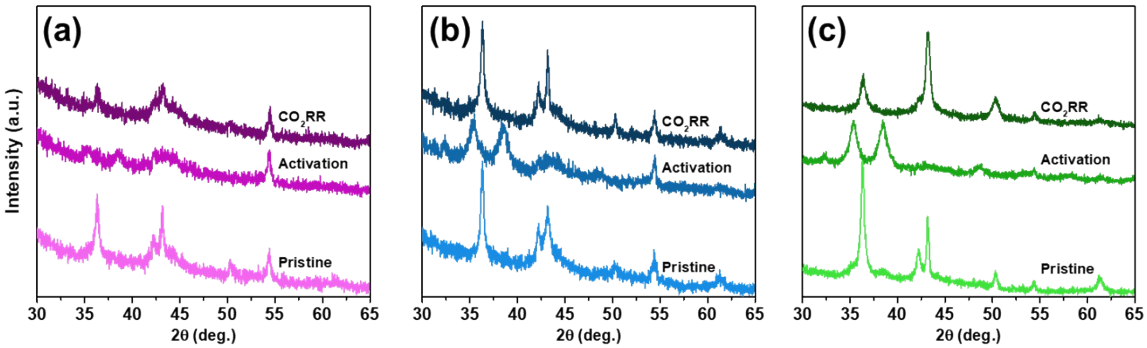


**Fig. S13** XRD spectra comparison of (a) cCu-5-1, (b) cCu-5-3, and (c) cCu-5-10 before and after the KOH treatment and the e$CO_2$RR.

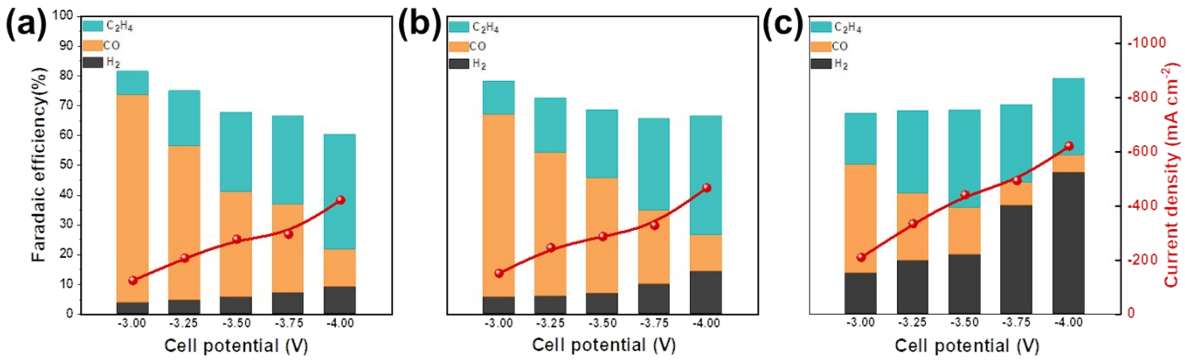


**Fig. S14** FEs of gaseous products and total current densities of (a) Cu-5-1, (b) Cu-5-3, and (c) Cu-5-10 depending on the applied cell voltages.

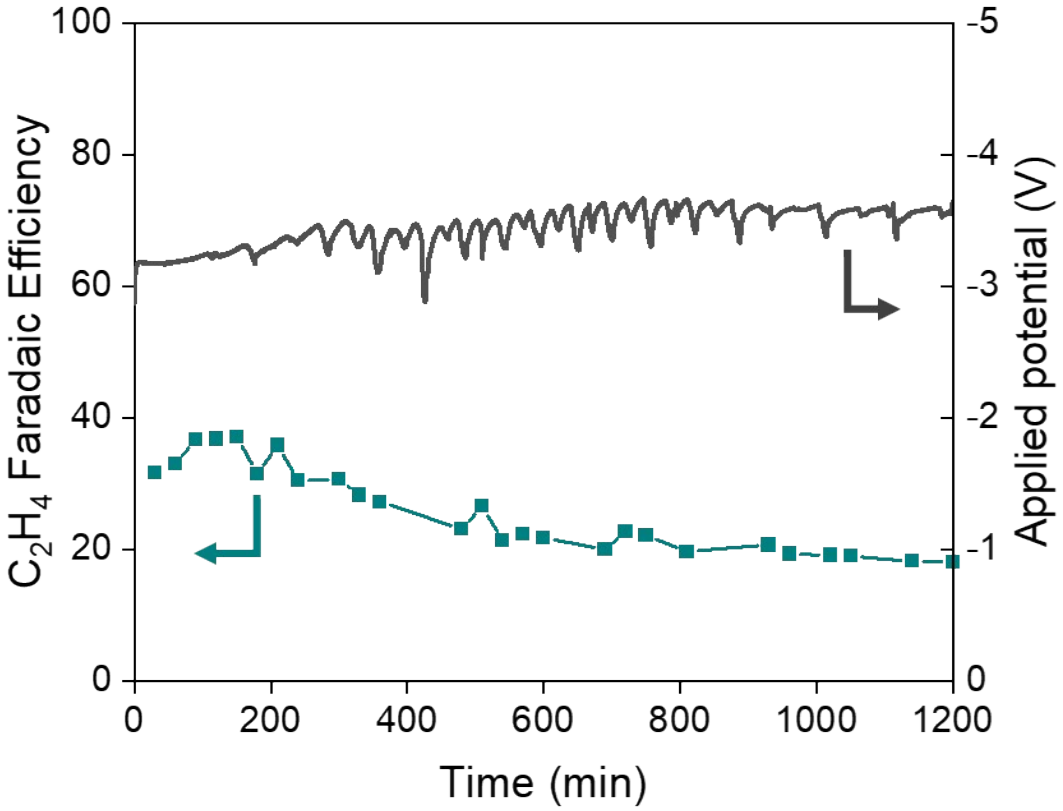


**Fig. S15** $C_2H_4$ FE and applied cell potential of Cu-5-3 catalyst electrode fixed current density of 300 mA $cm^{-2}$ during 20 h operation. Cu-5-3 catalyst was prepared by overlaying carbon black (ketjen black 600jd) and graphite powder adlayers to prevent a flooding and hydrophilic catalyst surface changes.

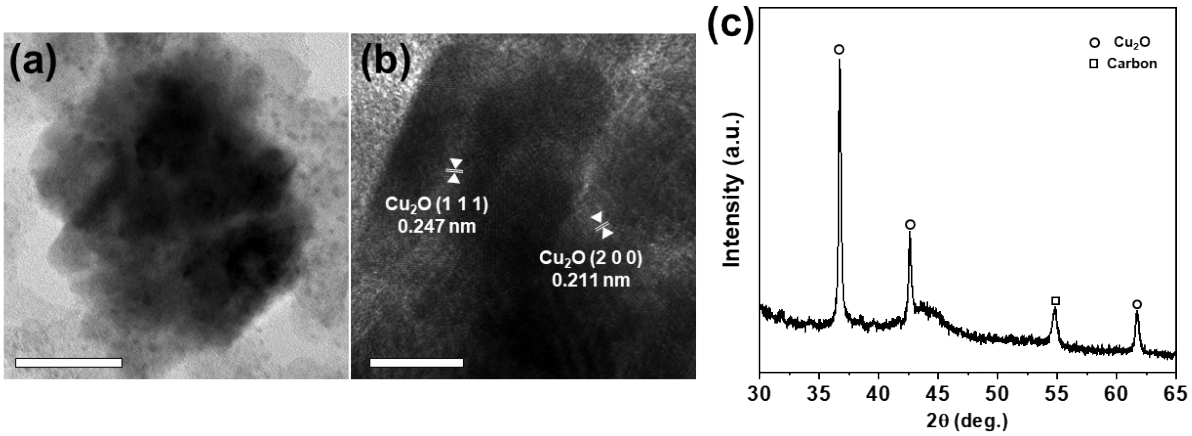


**Fig. S16** (a) TEM, (b) HRTEM, and (c) XRD spectrum of Cu-5 catalyst after 13 h stability test in the MEA cell at 300 mA $cm^{-2}$. The scale bars repsent (a) 50 nm and (b) 10 nm, respectively.

**Table S3** Summary and comparison of the $eCO_2RR$ performances in the catholyte-free MEA cell for $C_{2+}$ chemicals production

| # | Catalyst | FE(%) $H_2$ | FE(%) $C_{2+}$ chemicals | Voltage | $C_{2+}$ partial Current density (-mA $cm^{-2}$) | Ionomer | Membrane | Anolyte | Ref |
|---|---|---|---|---|---|---|---|---|---|
| | **Commercial Cu 25nm** | 14.7 | 67.3 | -3.85 V (cell voltage) | 336.5 | Sustainion | AEM | 0.1 M $KHCO_3$ | **This work** |
| 1 | $Cu_2O$ | 60 | 15 | 2.00 V (cell voltage) | 0.6 | — | AEM | — | 13 |
| 2 | $Cu_2O$ | — | 17 | 2.25 V (cell voltage) | 0.68 | — | AEM | $H_2O$ | 14 |
| 3 | Cu-CNF | — | 52 | 2.11 V (cell voltage) | 38.5 | Nafion | PEM | $H_2O$ | 15 |
| 4 | Porous PTFE + Cu(sputtering) + Carbon NPs + Graphite | <5 | 79 | -4.20 V (cell voltage) | 158 | — | AEM | 0.1 M $KHCO_3$ | 16 |
| 5 | Porous PTFE + CIBH | — | 50 | -3.90 V (cell voltage) | 347.2 | CIBH | AEM | 0.1 M $KHCO_3$ | 17 |
| 6 | Porous PTFE + modified Cu | — | 60 | 3.62 V (cell voltage) | 72 | — | AEM | 0.1 M $KHCO_3$ | 18 |
| 7 | Porous PTFE + Cu(sputtering) + CTPI | — | 69 | -4.40 V (cell voltage) | 303.6 | TP/SCC | AEM | 0.1 M $KHCO_3$ | 19 |
| 8 | Cu | <2 | <2 | -3.00 V (vs. 3 M Ag/AgCl) | <2.2 | Sustainion | AEM | 10 mM $KHCO_3$ | 20 |
| 9 | Cu | 89 | 11.8 | -1.70 V (vs. SCE) | 3.1 | — | PEM | 0.5 M $K_2SO_4$ | 21 |
| 10 | Cu-SPE | — | 10 | -2.00 V (vs. SCE) | 0.1~0.8 | — | PEM | 1 mM $H_2SO_4$ | 22 |
| 11 | Cu film | NC. | 45.5 | -0.60 V (vs. RHE) | 30.7 | — | Polymers | 1 M KOH | 23 |
| 12 | Cu-$SiO_x$ | — | 65 ($C_2H_4$) | -4.1 V (cell voltage) | 215 | Polymeric binder | AEM | 0.1 M $KHCO_3$ | 24 |
| 13 | Cu-KOH | — | 78.7 | -3.25 V (cell voltage) | 221 | Sustainion | AEM | 1 M KOH | 25 |
| 14 | Defect-rich Cu | — | 60 (ethanol, n-propanol) | -3.5 V (cell voltage) | 120 | Sustainion | AEM | 0.1 M $KHCO_3$ | 26 |
| 15 | Cu cube | 10 | 38.5 | -3.75 V (cell potential) | 90 | Sustainion | AEM | 0.1 M $KHCO_3$ | 27 |
| 16 | Sputtered Cu | 5 | 85 | -2.4 V (cell potential) | 102 | — | AEM | 0.1 M $KHCO_3$ | 28 |

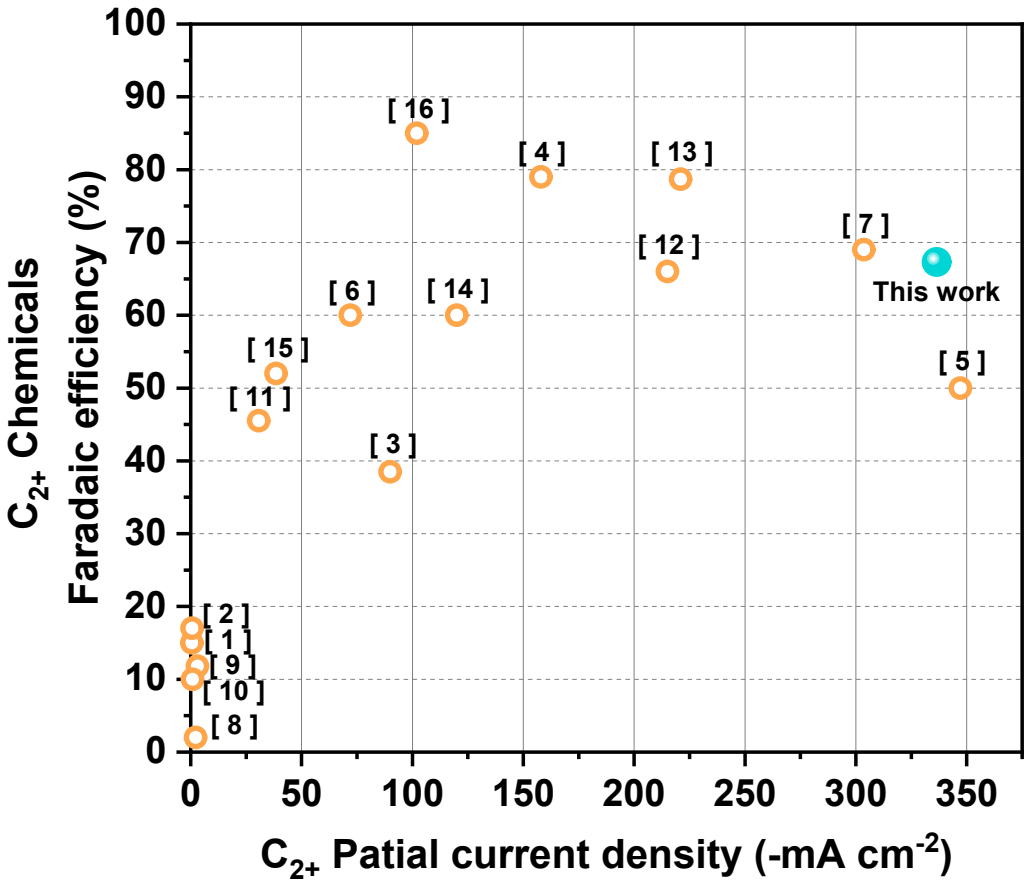


**Fig. S17** Summary and comparison of $eCO_2RR$ performances showing the partial current densities of the $C_{2+}$ chemicals (x-axis) and their FEs (y-axis) using Cu-based catalysts in the zero-gap and catholyte-free MEA cell.

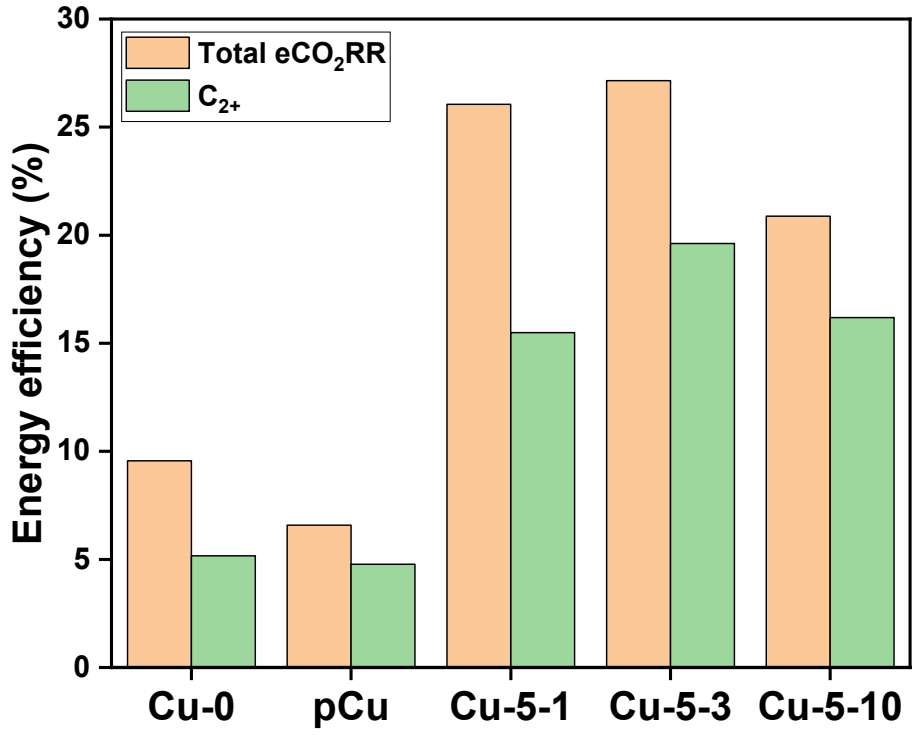


**Fig. S18** Total $eCO_2RR$ (orange) and $C_{2+}$ production (green) energy efficiencies of Cu-0, pCu, Cu-5-1, Cu-5-3, and Cu-5-10 at fixed current density of 500 mA $cm^{-2}$.

**Supplemental References**


1 O. A. Baturina, Q. Lu, M. A. Padilla, L. Xin, W. Li, A. Serov, K. Artyushkova, P. Atanassov, F. Xu, A. Epshteyn, T. Brintlinger, M. Schuette and G. E. Collins, *ACS Catal.*, 2014, **4**, 3682–3695.

2 L.-C. Weng, A. T. Bell and A. Z. Weber, *Energy Environ. Sci.*, 2020, **12**, 3592–3606.

3 D. L. T. Nguyen, C. W. Lee, J. Na, M. C. Kim, N. D. K. Tu, S. Y. Lee, Y. J. Sa, D. H. Won, H. S. Oh, H. Kim, B. K. Min, S. S. Han, U. Lee and Y. J. Hwang, *ACS Catal.*, 2020, **10**, 3222–3231.

4 Y. Lum, B. Yue, P. Lobaccaro, A. T. Bell and J. W. Ager, *J. Phys. Chem. C*, 2017, **121**, 14191–14203.

5 H. Erying and D. Henderson, *Theoretical Chemistry: Advances and Perspectives*, Academic Press, USA, 1975, pp. 177-234.

6 B. P. Sullivan, K. Krist and H. E. Guard, *Electrochemical and electrocatalytic reactions of carbon dioxide*, Elsevier Science, Netherlands, 1992.

7 L. C. Weng, A. T. Bell and A. Z. Weber, *Energy Environ. Sci.*, 2019, **12**, 1950–1968.

8 H. C. Brinkman, *J. Chem. Phys.*, 1952, **20**, 571.

9 B. Ghanbarian, A. G. Hunt, R. P. Ewing and M. Sahimi, *SSSA*, 2013, **77**, 1461-1477.

10 S. Ergun, *Chem. Eng. Prog.*, 1952, **48**, 89-94.

11 N. Gupta., M. Gattrell and B. MacDougall, *J. Appl. Electrochem*, 2006, **36**, 161-172.

12 E. L. Cussler, *Diffusion: mass transfer in fluid systems*, Cambridge University Press, England, 2009.

13 L. M. Aeshala, R. G. Uppaluri and A. Verma, *J. CO2 Util.*, 2013, **3**–**4**, 49–55.

14 L. M. Aeshala, R. Uppaluri and A. Verma, *Phys. Chem. Chem. Phys.*, 2014, **16**, 17588–17594.

15 N. Gutiérrez-Guerra, L. Moreno-López, J. C. Serrano-Ruiz, J. L. Valverde and A. de Lucas-Consuegra, *Appl. Catal. B Environ.*, 2016, **188**, 272–282.

16 C. M. Gabardo, C. P. O'Brien, J. P. Edwards, C. McCallum, Y. Xu, C. T. Dinh, J. Li, E. H. Sargent and D. Sinton, *Joule*, 2019, **3**, 2777–2791.

17 F. P. García de Arquer, C. T. Dinh, A. Ozden, J. Wicks, C. McCallum, A. R. Kirmani, D. H. Nam, C. Gabardo, A. Seifitokaldani, X. Wang, Y. C. Li, F. Li, J. Edwards, L. J. Richter, S. J. Thorpe, D. Sinton and E. H. Sargent, *Science*, 2020, **367**, 661–666.

18 F. Li, A. Thevenon, A. Rosas-hernández, Z. Wang, Y. Li, C. M. Gabardo, A. Ozden, C. T. Dinh, J. Li, Y. Wang, J. P. Edwards, Y. Xu, C. Mccallum, L. Tao, Z. Liang, M. Luo, X. Wang, H. Li, C. P. O. Brien, C. Tan, D. Nam, R. Quintero-bermudez, T. Zhuang, Y. C. Li, Z. Han, R. D. Britt, D. Sinton, T. Agapie, J. C. Peters and E. H. Sargent, *Nature*, 2020, **577**, 509–514.

19 A. Ozden, F. Li, F. P. GarcÍa De Arquer, A. Rosas-Hernández, A. Thevenon, Y. Wang, S. F. Hung, X. Wang, B. Chen, J. Li, J. Wicks, M. Luo, Z. Wang, T. Agapie, J. C. Peters, E. H. Sargent and D. Sinton, *ACS Energy Lett.*, 2020, **5**, 2811–2818.

20 J. Lee, J. Lim, C. W. Roh, H. S. Whang and H. Lee, *J. CO2 Util.*, 2019, **31**, 244–250.

21 S. Komatsu, M. Tanaka, A. Okumura and A. Kungi, *Electrochim. Acta*, 1995, **40**, 745–753

22 D. W. Dewulf and A. J. Bard, Catal. Letters, 1988, **11**, 73-79.

23 S. C. Perry, S. M. Gateman, R. Malpass-Evans, N. McKeown, M. Wegener, P. Nazarovs, J. Mauzeroll, L. Wang and C. Ponce de León, *Chemosphere*, 2020, **248**, 125993.

24 J. Li, A. Ozden, M. Wan, Y. Hu, F. Li, Y. Wang, R. R. Zamani, D. Ren, Z. Wang, Y. Xu, D. H. Nam, J. Wicks, B. Chen, X. Wang, M. Luo, M. Graetzel, F. Che, E. H. Sargent and D. Sinton, *Nat. Commun.*, 2021, **12**, 2808.

25 W. H. Lee, C. Lim, S. Y. Lee, K. H. Chae, C. H. Choi, U. Lee, B. K. Min, Y. J. Hwang and H. S. Oh, *Nano Energy*, 2021, **84**, 105859.
26 Z. Gu, H. Shen, Z. Chen, Y. Yang, C. Yang, Y. Ji, Y. Wang, C. Zhu, J. Liu, J. Li, T. K. Sham, X. Xu and G. Zheng, *Joule*, 2021, **5**, 429–440.
27 G. O. Larrazábal, V. Okatenko, I. Chorkendorff, R. Buonsanti and B. Seger, *ACS Appl. Mater. Interfaces*, 2022, **14**, 7779-7787.
28 G. Zhang, Z. J. Zhao, D. Cheng, H. Li, J. Yu, Q. Wang, H. Gao, J. Guo, H. Wang, G. A. Ozin, T. Wang and J. Gong, *Nat. Commun.*, 2021, **12**, 5745.